International Journal of Fatigue 184 (2024) 108332

Contents lists available at ScienceDirect

International Journal of Fatigue

journal homepage: www.elsevier.com/locate/ijfatigue

Study of fatigue crack propagation on modified CT specimens under variable amplitude loadings using machine learning

B. Santos [a], V. Infante [b,*], T. Barros [a], R. Baptista [b,c]

[a] Academia da Força Aérea, Granja do Marquês, 2715-021 Pêro Pinheiro, Portugal
[b] LAETA, IDMEC, Instituto Superior Técnico, Universidade de Lisboa, Av. Rovisco Pais, 1049-001 Lisboa, Portugal
[c] UnIRE, Instituto Superior de Engenharia de Lisboa, Instituto Politécnico de Lisboa, R. Conselheiro Emídio Navarro 1, 1959-007 Lisboa, Portugal

ARTICLE INFO

Keywords:
Modified CT Specimens
Fatigue Crack Propagation
Finite Element Analysis
Variable Amplitude Fatigue
Machine Learning

ABSTRACT

This study focuses on predicting fatigue crack paths and fatigue life in modified compact tension specimens, under mixed mode and variable amplitude loading conditions, using Machine Learning techniques. Mixed-mode conditions were induced by using specimens that incorporated holes with different radii and center coordinates. Initially, multiple Finite Element Method (FEM) simulations were conducted to determine the fatigue crack path for different configurations. Subsequently, several configurations were selected for experimental fatigue testing, in which the fatigue crack path was monitored and recorded. The final phase of the study involved Machine Learning (ML) techniques, specifically Artificial Neural Networks (ANN) and k-Nearest Neighbors (kNN), to predict fatigue crack propagation. The models were trained using different numerical and experimental data. Predicted results were then compared with experimentally tested data, and the behavior and accuracy of the models were evaluated. Overall, the implemented models demonstrated the ability to predict fatigue crack path with average deviations (ANN – 1.19 mm; kNN – 1.10 mm) closely resembling results obtained through Finite Element simulations (1.65 mm). The models were also able to predict fatigue life with average errors of 10.1 % (ANN) and 16.7 % (kNN), all achieved with a reduction of computational costs greater than 90 %.

1. Introduction

The prevalence of fatigue-related issues causing mechanical failures in aeronautical components originates a compelling need to intensify research efforts, especially in variable amplitude scenarios [1]. Simultaneously, developing innovative and efficient tools that minimize human and computational workloads is a paramount goal. Given these considerations, leveraging Machine Learning (ML) methods to predict materials' behavior under variable amplitude fatigue conditions has gained significant interest. As ML has become an increasingly powerful tool, its application in solving complex problems in various fields has grown, and the field of mechanical behavior of materials was no exception [2].

Fatigue crack growth under mixed mode conditions is an especially complex problem to analyze [3]. Mixed mode conditions can be introduced due to loading modes or specimen geometry. Under complex tensile and shear loading modes, crack propagation leads to crack deflection that can be predicted using different propagation criteria, such as the maximum tangential stress criterion (MTS) (tensile mode) typically for tensile dominated proportional loading, or the maximum shear stress criterion (MSS) (shear mode) for shear dominated and non-proportional loading conditions [4,5,6]. Notches, holes and other geometrical design details can also deflect crack propagation [7] due to mixed mode conditions on the crack front. While the previous criteria, based on the stress intensity factors (SIF), can predict crack propagation angles for tensile and shear modes, Floros et al. have concluded that more advance criteria, like the vector crack tip displacement (VCTD), can actually predict the transitions between these modes [8]. Therefore, to simulate fatigue crack growth numerically, one must determine the SIF or the displacement fields around the crack tip. This data can be calculated using the finite element method (FEM) [9]. Unfortunately, it must be updated as the crack length increases, taking into consideration the new crack propagation direction. While meshless methods, as the eXtended finite element method (XFEM), allow for easy numerical crack propagation analysis [10], automated crack propagation algorithms, allow for automatic remeshing of the simulated component, adapting the mesh to the update crack configuration and enabling for enhance results [11].[911].

* Corresponding author.
E-mail address: virginia.infante@tecnico.ulisboa.pt (V. Infante).

https://doi.org/10.1016/j.ijfatigue.2024.108332
Received 8 February 2024; Received in revised form 1 April 2024; Accepted 12 April 2024
Available online 15 April 2024

Extensive numerical calculations require time and computational power, therefore, training new ML tools may be a solution, that can offer instantaneous fatigue crack propagation and life data. In 2017, Wang et al. [12] implemented three different ML algorithms intending to calculate fatigue crack propagation rates. The algorithms used were the extreme learning machine (ELM), the radial basis function network (RBFN), and the genetic algorithms of optimized backpropagation network (GABP). The predictions from these algorithms were compared with experimental data, and they exhibited high-quality performance in all three methods. Another important observation was that the effectiveness of this method is closely linked to the amount and quality of the experimental data available. Also, in crack propagation, Mortazavi et al. [13] managed to predict FCG rates in the short and long-crack regimes by applying artificial neural networks (ANN). Despite the limited data conditions, the performance obtained was very satisfactory. The conclusions again state that the data's density, distribution, and accuracy are fundamental for correct implementation. In 2020, X. Liu et al. [14] concluded that ML solutions will change the way that engineering problems are solved, in a study to determine the fracture toughness of a specific material using Decision Trees and ANN. In the same study, the author lists four basic steps necessary to develop a ML model applied to fracture mechanics: i) problem definition, ii) preparation of the data set, iii) model selection, and iv) training and deployment of ML solutions. Problem definition is very important, as the selection of input and output variables will influence the ML performance [15], several authors consider the use of the Pearson correlation coefficient an effective way to ascertain the optimal variable selection [16]. The preparation of the data set is also very important, namely its quality and quantity. For crack propagation problems the data quality is represented by the training data definition. Wang and Shi recommend that a minimum of 0.5 mm crack increment is required to accurately represent crack propagation [3,10]. While the necessary data quantity is related with the number of input variables [17]. Zhao et al. also mentions that the ML model is very important for the final outcome. These authors used both feedforward neural networks to predict specimens fatigue life and long short-term memory neural networks to predict crack propagations paths, stating that the data nature influences the best model to be used [17].

Several studies have been carried out in the field of fracture mechanics applied to the prediction of fatigue crack trajectories in the last decade. The common objective of these studies was to determine the path of modified standard specimen.ANN was the most applied ML method, and the results were acceptable [3,15,18]. In 2021, Wang et al. [3] used RBFN to simulate fatigue crack propagation on modified CT specimens and on plates with double-holes. The networks were trained from both numerical and experimental data. These authors main conclusion was that is possible to train crack propagation and life predictions from a small amount of data, using only the limit values of the considered variables, the key is to optimize the input variable selection. More recently, in 2022, Baptista et al. [19] used Artificial Neural Networks (ANN) to predict fatigue crack growth in modified Compact Tension (CT) specimens. The results were compared with numerical simulations. The model performed well in predicting the crack path and showed excellent performance in determining whether the crack converged on the hole. While Wang et al used the relative position and direction between the crack and the hole, Baptista et al. used the hole global position and radius as input variables. In both cases the output chosen variables were the crack increment in both x and y directions. Baptista et al. were able to predict crack propagation more accurately, also due to the optimized ANN structure. The authors also noted the need for experimental testing to validate the model.

Even when the available data from ML is small authors like Liang et al. [20] or Zhao et al. [17] were able to accurately predict fatigue behavior by using data augmentation techniques like linear, nearest neighbor, natural neighbor, and cubic spline interpolations. This fundamentally allows to avoid problems such as overfitting and underfitting. Overfitting can occur when only a small amount of data is available for training, or when ML models have a large number of parameters and degrees of freedom. While underfitting occurs when the ML tool is not able to learn the required behavior, due to the small training data set. Chen et al. [21] have also tried to solve these issues by combining physical and ML models. This allows to accommodate multi-fidelity data from both numerical or experimental and physical model origin, in the hybrid tool. Their main conclusion is that these hybrid models can produce more accurate results, when compared against simple ANN, random forest, or support vector machines. Liu and Fan [16,22] have also used physics integrated models for very high cycle fatigue life predictions. In this case, the introduction of a Z-parameter, informing the model about the fatigue defect size, location and stress amplitude, allowed for more accurate predictions even when the training data size was small. These authors also proposed a method for data expansion based on the Z-parameter: a) using the experimental data to empirically determine the Z-parameter equations; b) chaging the value of one independent variable to generate a set of expanded data; and c) repeat for all independent variables. Properly expanding the training data set was essential to accurately train the model.Other authors as Gope et al. [15] and Wang et al. [3] have also related the solution for this problem on the optimal selection of the input variables and the learning rate, stating that higher learning rates allow for better crack propagation angle predictions. Overall, a well optimized ML tool, with sufficient data for training, well-selected input variables and well-designed structure may allow for a computational efficiency of at least 30 % higher than other numerical solutions [23,24]. This is achieved by reducing the overall number of numerical simulations need to fully understand the problem behavior [17]. ML will provide tools for real time fatigue assessment and prediction, once properly trained [25].

The main objective of this study is to predict fatigue crack paths and fatigue life under variable amplitude loading and mixed-mode conditions using ML techniques. Additionally, the framework and procedures for investigating fatigue phenomena experimentally in adherence to scientific standards and best practices have been established. The research involved the application of ML models capable of predicting fatigue crack propagation paths based on component geometry and fatigue life under typical flight loads. Experimental tests were conducted to assess and validate the developed ML models. The research aimed to create advanced and cost-effective ML tools, incorporating experimental data to enhance understanding fatigue crack propagation in aeronautical components.

2. Materials and methods

2.1. Modified compact tension specimen

To achieve the research objectives, modified CT specimens were employed. The geometry and dimensions (as depicted in Fig. 1) were defined in agreement with ASTM E647 [26]. The specimens were modified to include an additional hole in the upper region, illustrated in Fig. 2.

2.2. Variables of interest

Consequently, the study established five variables of interest, including X_{cf} and Y_{cf} representing the coordinates of the crack front, X_{hole} and Y_{hole} denoting the coordinates of the hole, along with R_{hole}, which signified the hole's radius. The specific coordinates and size limits for the hole can be found in Table 1. Constraining the problem variables is essential to maintain the study within manageable dimensions and the domain was carefully defined to encompass sink hole and miss hole scenarios for all specified radii. The area encompassing all possible localizations of additional hole's center is presented in Fig. 3.

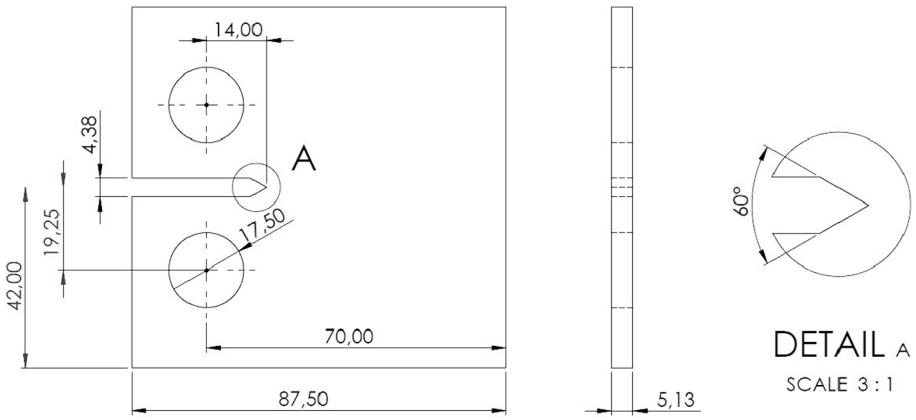

Fig. 1. Geometry and dimensions of employed CT specimens.

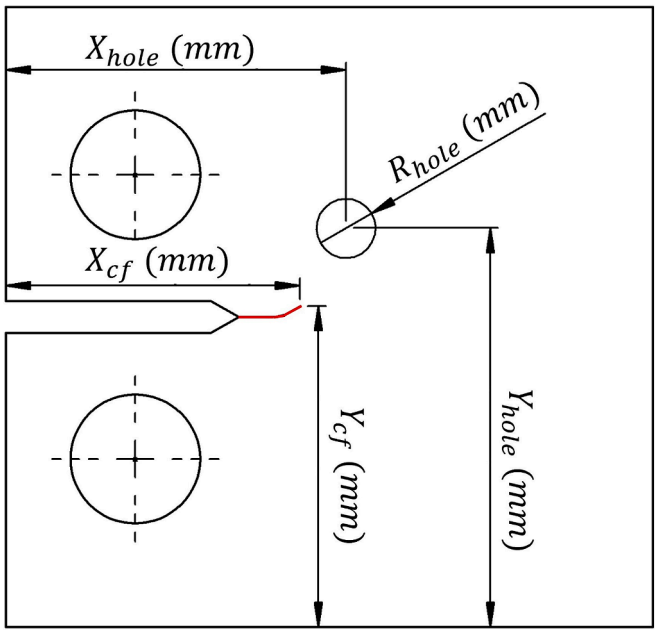

Fig. 2. Graphical representation of the variables of interest on the modified CT specimens.

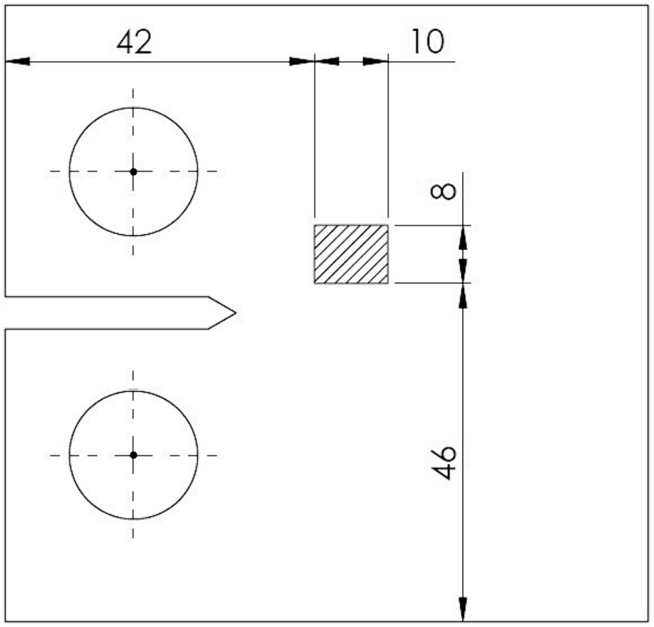

Fig. 3. The domain of the additional hole's center.

Table 1
The domain of the variables regarding additional hole.

Variable	Min. value [mm]	Max. value [mm]
X_{hole}	42	52
Y_{hole}	46	54
R_{hole}	3	5

Table 2
Mechanical properties of aluminum alloy 2024-T3.

Property	Value
Yield Stress (0.2%-offset) [MPa]	338
Ultimate Strength [MPa]	472
Total Elongation [%]	22
Young's Modulus [GPa]	73.1
Poisson Ratio	0.33

2.3. Specimen material

The material selection leaned towards the 2024-T3 aluminum alloy, a well-established choice in aerospace applications, particularly in the TB-30 Epsilon aircraft. The documentation and research available on this material further supported this choice. Table 2 provides an overview of material properties, encompassing various mechanical characteristics.

2.4. Flight spectrum

In order to forecast fatigue life under varying amplitude loads, a specific load spectrum was chosen from real flight Load Factor (LF) spectra of the PrtAF Epsilon TB-30 [27]. This spectrum, depicted in Fig. 4, was selected due to its severity, which expedited the experiments, and its absence of negative load factors, a requirement based on the specimen's clamping configuration. This spectrum ensured the experimentally tested specimens encountered realistic variable amplitude loading conditions, providing insights into the material's fatigue response in complex scenarios.

The spectrum has undergone a linear transformation from load factor to applied force. The linear transformation is shown in eq. (1) and takes each load factor (already normalized) and returns the force to be applied

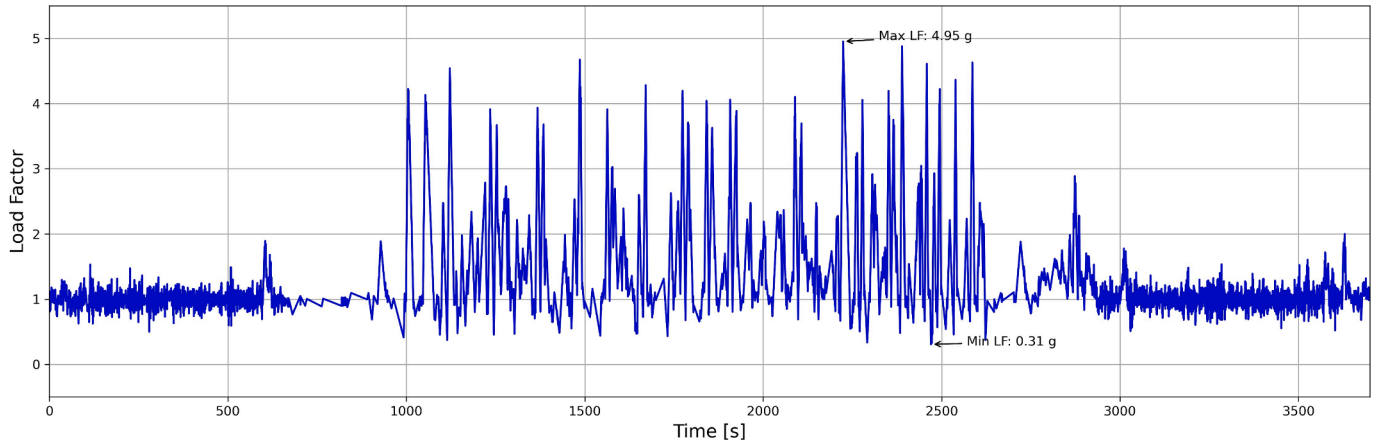

Fig. 4. Flight spectrum used in the study.

to the specimen. Two constants, 5000 N, and 6500 N, were used. The 5000 N value was used for a single test solely to validate crack propagation models. The addition of 500 N in the final part of the transformation was related to the testing equipment's clamping system.

$$Load = \frac{LF}{\max(LF)} \times P + 500[N], P = \{5000, 6500\} \quad (1)$$

2.5. Numerical methodology

The methodology adopted in this study is described in Fig. 5. Initially Finite Element Method (FEM) simulations were performed, providing a first look into the phenomenon under investigation. On the simulated cracked specimens, the crack was allowed to propagate, and stress intensity factor (SIF) vs crack length (a) curves were obtained, along with the corresponding crack paths. Then, the available specimens were categorized into two groups for experimental tests. The first group, unmodified specimens, validated the fatigue crack growth algorithm for variable amplitude and its propagation models. The second group, featuring specimens with modified additional holes, was used to study crack paths, and compared results with FEM data. Finally, data from FEM simulations and experimental tests were combined to create different datasets. These datasets used data from both numerical simulations and experimental testing. ML models were developed to predict fatigue crack paths and fatigue life. Model performance was retrieved by comparing results with experimental data.

The automatic crack propagation algorithm leveraged FEM to evaluate crack development. This algorithm was inspired by the work of Batista et al. [19] and it is presented in Fig. 6. The individual steps will be briefly explained in the following paragraphs.

The initial step involves defining the location and radius of the additional hole, which dictated the path of the crack. In the geometry definition phase, a virtual representation of the structure is established using *ABAQUS CAE*. Subsequently, the crack's path was delineated by converting discrete points into a continuous line. As the crack propagates, this integrated line will be updated dynamically. Material properties, including modulus of elasticity and Poisson's ratio, are defined in the next step. Specifying these properties allows an accurate replication of real-world material behavior. In the following step, the simulation replicated the experimental conditions by defining applied loads, which consisted of symmetrical vertical forces toward the clamping hole center. Boundary conditions involved coupling the *y*-displacements of the hole centers and their defining circumferences, along with restricting movement in the *x* direction for these holes. The mesh generation step employed a dual approach for efficient meshing, as depicted in Fig. 7. It utilized a refined mesh with 6-node Modified Linear Triangle (*CPS6M*) elements near the crack front to capture stress singularity accurately. Simultaneously, a coarser mesh configuration with 8-node Reduced Integration Linear Brick (*CPS8R*) elements was applied in distant areas for improved computational efficiency while maintaining precision. In the subsequent phase, a static analysis was conducted to determine the SIF. By simulating the structure under static conditions, the algorithm extracts the necessary fracture mechanics parameters, namely both SIF for mode I and II (K_I and K_{II}), which were crucial for understanding the

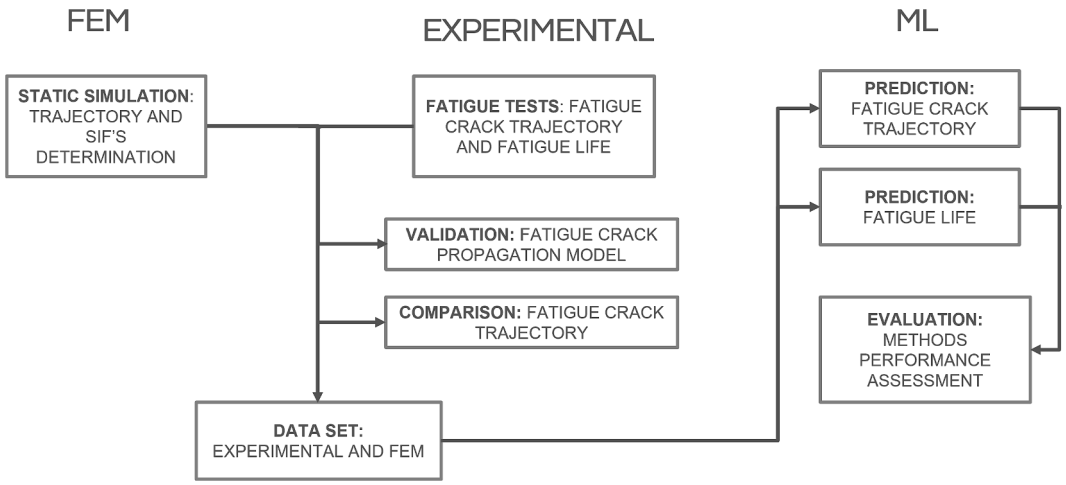

Fig. 5. Overall methodology applied on the study.

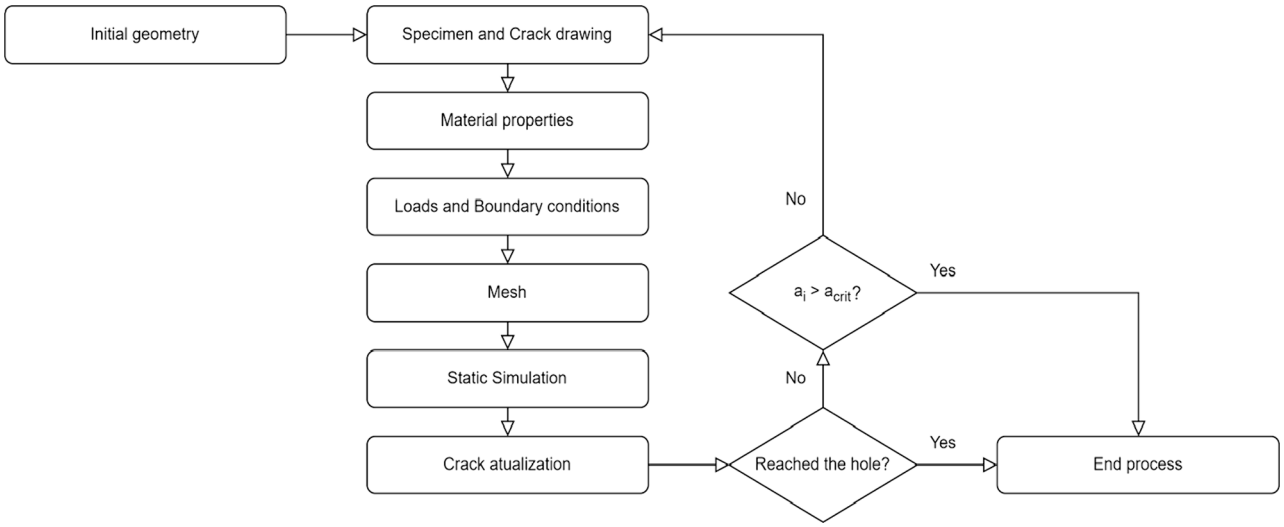

Fig. 6. Automatic crack propagation algorithm [19].

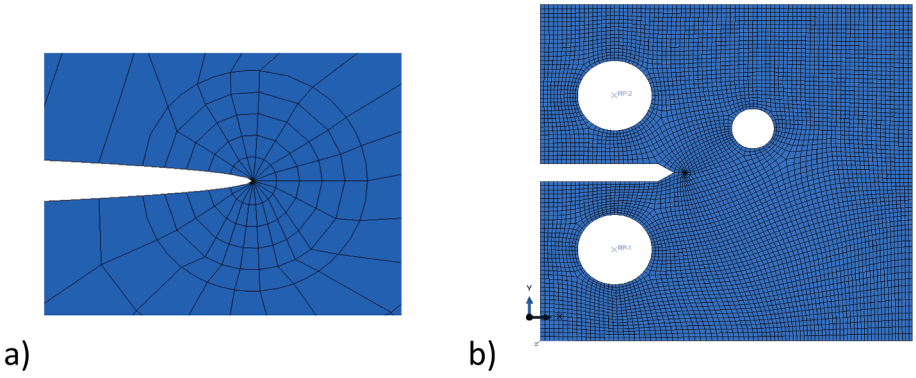

Fig. 7. Generated mesh: a) CPS6M fan-shaped elements near the crack; b) CPS8R elements on outside regions.

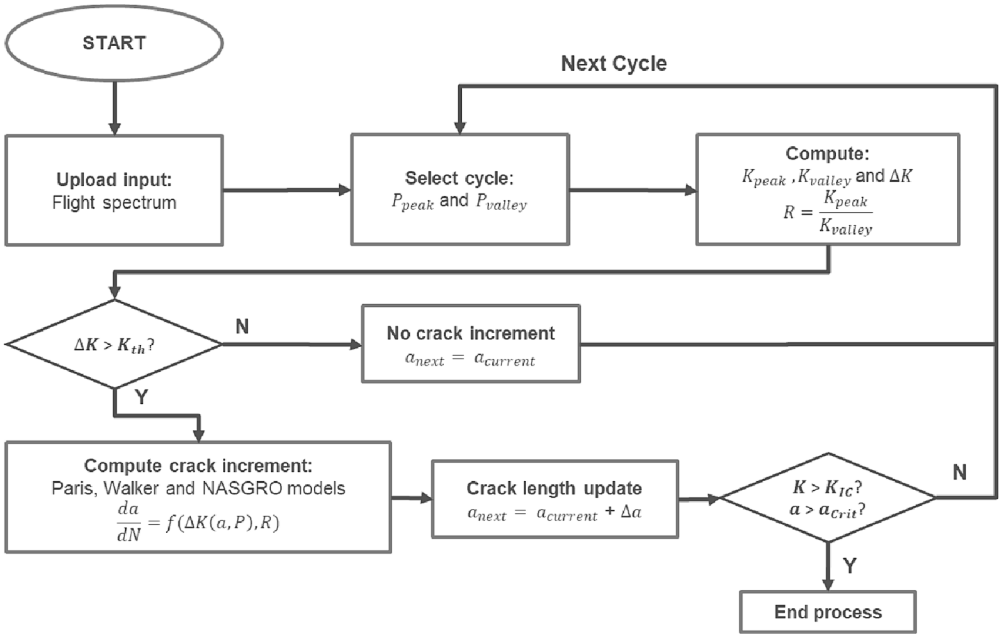

Fig. 8. Flowchart describing the algorithm implemented for crack propagation under variable amplitude loading [28].

structure's susceptibility to crack propagation.

Using the obtained SIF, the algorithm calculates the crack's propagation angle, following the MTS criterion [19] (eq.(2)), a well-established orientation criterion supported by existing fatigue propagation research. Afterward, the crack's path was incrementally updated with a fixed length, with the direction updated by the calculated angle.

$$\theta = 2tan^{-1}\left(\frac{1}{4}\left(\frac{K_I}{K_{II}} \pm \sqrt{\left(\frac{K_I}{K_{II}}\right)^2 + 8}\right)\right) \tag{2}$$

Subsequent to the update, two conditions must be met: the crack should not have reached the hole or its critical length. The process was concluded when either of these conditions was satisfied.

The crack propagation algorithm previously discussed offered insights into path and SIF but lacked the capability to predict crack growth under variable amplitude loading. In order to address this, a procedure was devised to assess damage from individual loading cycles and accumulate it to establish the crack growth curve over cycles. This procedure drew inspiration from the work of Barros et al. [28] and is illustrated in Fig 8.

Three fatigue crack propagation models were employed to compute the infinitesimal crack bedegrowth increment: Paris Law [29], Walker Law [29], and NASGRO equation [30,31]. The Paris law [29], expressed by Eq. (3), exclusively relies on the ΔK value for increment determination.

$$\frac{da}{dN} = C\Delta K^m \tag{3}$$

In contrast, Walker's law [29], represented by Eq. (4), incorporates the R-Ratio value, defined as the ratio between K_{valley} and K_{peak}.

$$\frac{da}{dN} = C_W\overline{\Delta K}^{n_w} = C_W\left[\frac{\Delta K}{(1-R)^{1-\gamma}}\right]^{n_w} \tag{4}$$

The NASGRO equation [31,30], presented in Eq. (5), stands as the most thorough of the three, as it includes the Newman crack closure function, f, the non-propagation limit, denoted as K_{th}, and the critical stress intensity factor, K_{crit}.

$$\frac{da}{dN} = C_N\left[\frac{1-f}{1-R}\Delta K\right]^{n_N}\frac{\left(1-\frac{\Delta K_{th}}{\Delta K}\right)^p}{\left(1-\frac{\Delta K_{max}}{K_{crit}}\right)^q} \tag{5}$$

The constants within the fatigue crack propagation models require experimental determination and are material specific. Previous research conducted by Martins et al. [32] established these constants for the aluminum alloy 2024-T3, and their values are detailed in Table 3.

2.6. Experimental methodology

Ten different specimens' configurations were used in experimental tests. Two specimens without an additional hole served as baseline cases to evaluate propagation models, while the remaining eight featured holes of varying radii (3 mm, 4 mm, or 5 mm), with Table 4 providing information on hole positions, radii, applied forces, and expected crack behaviors based on FEM analysis.

Table 3
Material properties for different propagation laws, obtained for be Aluminium alloy 2024-T3 [32].

Paris		Walker		NASGRO	
Parameter	Value	Parameter	Value	Parameter	Value
C_P	3.4×10^{-11}	C_W	2.6×10^{-11}	C_N	2.7×10^{-9}
n_P	3.6	n_W	3.6	n_N	1.8
		γ	0.21	p	1
				q	1

Table 4
CT specimens' configuration used in experimental tests.

Specimen	a_0 [mm]	x_h [mm]	y_h [mm]	r_h [mm]	P [N]	Type
CT1	16	–	–	–	5000	no hole
CT2	16	–	–	–	6500	no hole
CT3	16	47.0	47.0	3	6500	sink hole
CT4	16	48.0	52.5	3	6500	miss hole
CT5	16	42.0	50.0	4	6500	sink hole
CT6	16	52.0	50.0	4	6500	sink hole
CT7	16	48.0	54.0	4	6500	miss hole
CT8	16	45.5	49.5	5	6500	sink hole
CT9	16	48.5	48.5	5	6500	sink hole
CT10	16	50.0	52.0	5	6500	sink hole

The experimental procedure was divided into sequential stages, as presented in Fig. 9. For the fatigue tests, a pre-cracking procedure was crucial for standardizing the initial crack conditions and reducing discrepancies in notch sharpness introduced during manufacturing. This process involved applying a cyclic load of constant amplitude to reach the desired initial crack length, using a load magnitude set as a percentage of the maximum load for the subsequent variable amplitude test. Standard practice dictates that this percentage should fall between 50 % and 80 %, with reduced R ratio values.

The pre-cracking was performed until the crack length reached a final value of 2 mm with an allowable 0.1 mm difference. Table 5 provides a record of the cycles needed to reach the initial crack size, underlining the significance of this procedure.

During fatigue tests, periodic crack length measurements were taken as a function of the number of cycles applied from the start of the test. After completing the test, each specimen was analyzed to obtain the path of the crack front. An algorithm was devised to convert the irregularly spaced experimental path points into a structured set with consistent 0.5 mm intervals that match the FEM data. Figs. 10 and 11 present a graphical representation of those measurements.

2.7. Machine learning procedure

Before developing predictive models, the study proceeded through a feature engineering phase. During this phase, it was observed that the variables of the hole position remained constant within a particular configuration, which could potentially hinder the performance of ML models. To overcome this, variables representing the crack front and additional hole center positions were unified into a pair of variables, ΔX and ΔY, presented in Eqs. (6) and (7). These new variables quantified the differences between the two positions and ensured the tool's applicability no longer relied on fixed reference points but rather a relative framework.

$$\Delta X = X_{hole} - X_{crack} \tag{6}$$

$$\Delta Y = Y_{hole} - Y_{crack} \tag{7}$$

Subsequently, an analysis of all variables (both new and existing) was conducted to determine which ones held the most significant influence in predicting both ϑ and K_I. The findings were as follows:

- For ϑ_{next} prediction, the input variables were ΔX, ΔY, R_{hole}, ϑ_{prev} and a.
- For K_I prediction, the input variables were X_{crack}, Y_{crack}, ΔX, ϑ_{prev} and a.

The implementation of each model encompassed the following sequential steps: Scaling, Data Set Definition, Architecture Specification, Training, and Testing, followed by Performance Evaluation.

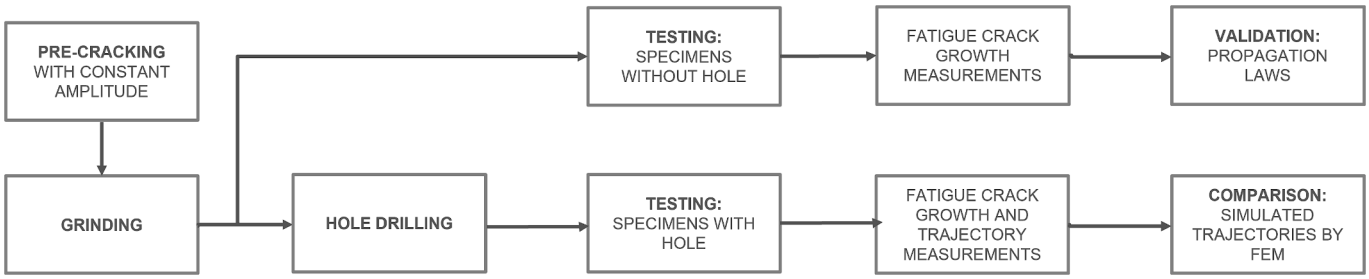

Fig. 9. Experimental procedure flow-chart.

Table 5
Number of pre-crack cycles and initial crack length of each specimen.

CT1	CT2	C31	CT4	CT5	CT6	CT7	CT8	CT9	CT10
a_i [*mm*] 1.913	1.958	2.023	1.956	1.969	2.013	1.937	1.961	1.982	1.995
Cycles100 000	128 000	67 850	48 000	62 000	52 000	56 000	54 000	92 000	50 000

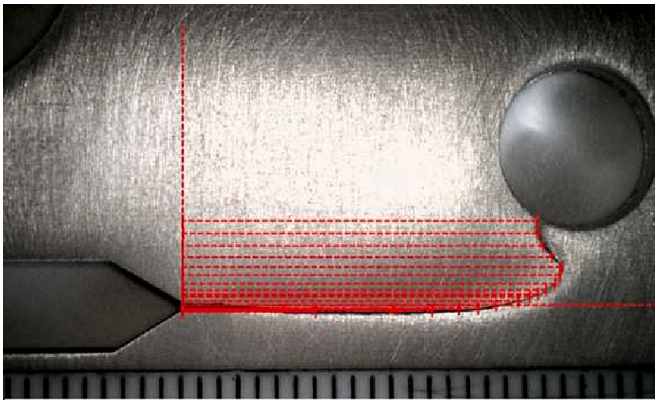

Fig. 10. Crack length measurement of CT5 specimen after 457 800 cycles.

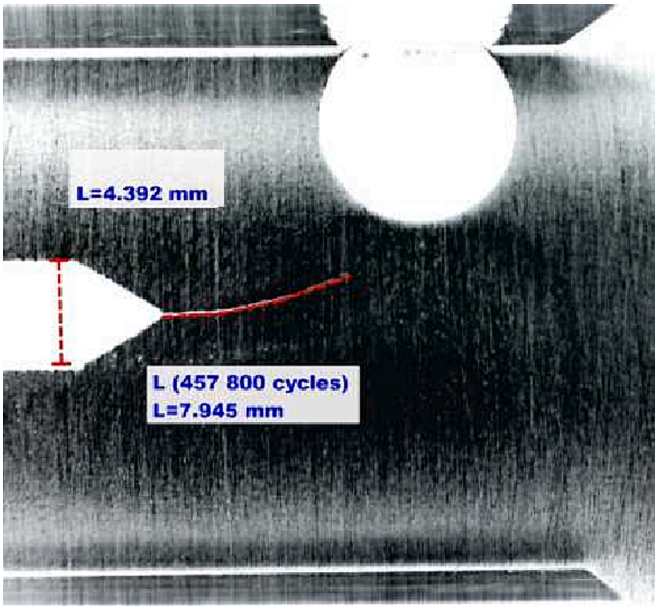

Fig. 11. Discretized path points and their measurements.

Scaling was a preprocessing step that ensured that variables were brought to a standard scale, preventing certain features from dominating the learning process and thus enhancing the model's performance.

Differences arose in the Data Set definition, particularly between the models predicting ϑ and K_I. in order to predict the crack propagation angle, ϑ_{next}, six different approaches were employed in constructing the training dataset to investigate the impact of data source and quantity on model performance, as presented in Table 6. The creation of these six distinct approaches aimed to investigate the influence of the quantity and type of data (experimental and numerical) on model performance. Thus, two datasets consist of only four cases, one containing solely numerical data and the other exclusively experimental. Subsequently, two datasets comprise eight cases, one purely numerical and the other a combination of data from both groups. Finally, there are two larger datasets (20 and 50 cases) consisting solely of numerical data.

Out of the seven available experimental cases, four (CT3, CT5, CT7, and CT9) were chosen for integration into the training datasets, while the remaining three (CT4, CT6, and CT8) were reserved for evaluating the models' performance. The selection was made randomly despite having two constraints. Each dataset should have at least one case of each hole size, and the training dataset should be larger than the validation dataset.

Regarding K_I prediction, the absence of experimental data for training led to a single-defined approach using purely numerical data with twenty cases. Conversely, for the testing dataset, the seven experimental configurations, along with two other numerical cases, were employed.

The architecture of the ANN models is detailed in Table 7, and the training was conducted over 600 epochs.

Regarding kNN, it was determined to use the three nearest neighbors, the Euclidean distance metric for similarity measurement, and the subsequent computation of predictions by averaging the target values of these three closest neighbors.

After model development, the performance assessment was performed. For θ_{next}, the evaluation considered the path image and the maximum error. Regarding fatigue life, the initial assessment focused on comparing K_I concerning crack length using other simulated data, followed by an evaluation of crack propagation regarding the number of cycles until failure.

Table 6
Number of experimental and numerical cases in each approach.

Approach	A	B	C	D	E	F
Experimental Cases	4	0	4	0	0	0
Numerical Cases	0	4	4	8	20	50

Table 7
Configuration and parameters to define the hidden layers of the θ_{next} and K_I prediction models.

Hidden layer	Neurons		Activation function	Dropout		Regularizer	
	θ_{next}	K_I		θ_{next}	K_I	θ_{next}	K_I
1	200	400	ReLU	0.4	0.3	–	–
2	200	300	ReLU	0.4	0.35	L2 – 0.02	L2 – 0.1
3	200	250	ReLU	0.4	0.4	L2 – 0.02	L2 – 0.1
4	150	150	ReLU	0.4	0.25	L2 – 0.02	L2 – 0.1

3. Results and Discussion

The "Results and Discussion" section reviews three main issues: numerical simulations, experimental tests and machine learning predictions.

3.1. Numerical simulations

The procedure explained in 2.5. enabled obtaining the trajectories and evolutions of the SIF for all considered configuration. Fig. 12 displays the Von Mises stress field obtained from six different iterations of a complete simulation, providing insight into the evolution occurring in an automatic crack propagation process. The images were captured with a spacing of 3 mm of crack length.

As mentioned, the iterative process updates the crack with a fixed-length increment. Four different values were used to determine the best increment value, and a specific geometry was simulated to check the path while determining the time spent in each simulation. The tested values were 2 mm, 1 mm, 0.5 mm, and 0.3 mm. The results of the four simulations performed are shown in Fig. 13.

As can be observed, the differences at the end of the path are considerable when comparing the three largest increment sizes (2.0, 1.0 and 0.5 mm). Quantitatively, the value of x-coordinate at the point where the path intersects the hole in the four simulations can be observed from Table 8. It can be concluded that beyond 0.5 mm, the improvement in the simulation is negligible, while the computational cost increases considerably. This size is also repeatedly adopted in papers within the field [3,19]. The value of 0.5 mm was therefore chosen for the increment in automatic crack propagation algorithm.

The validation of the results obtained through the FEM was a fundamental aspect of ensuring the fidelity and reliability of predictions. In this pursuit, the outcomes of the FEM model were benchmarked against the predictive insights derived from two empirical models [26,33]. The comparison was made through the evolution of K_I along the length of the crack. Due to its specific nature, the literature did not provide empirical models of modified CT specimens, so it was necessary to resort to a FEM simulation of a standard configuration.

The first empirical model comes from the E647 standard [26], used to standardise experimental procedures in the field of fatigue. Eq. (8) shows the evolution of K_I as a function of the applied force P, the thickness b, the width w and the parameter α, which corresponds to the a/w ratio.

$$K_I = \frac{P}{b\sqrt{w}} \frac{(2+\alpha)}{(1-\alpha)^{\frac{3}{2}}} \left(0.886 + 4.64\alpha - 13.32\alpha^2 + 14.72\alpha^3 - 5.6\alpha^4\right) \tag{8}$$

The other model is taken from "The Stress Analysis of Cracks Handbook" [33], a compendium of expressions relating SIF to crack length for numerous crack types and configurations. The equation for a CT specimen, shown in Eq. (9), is referred to by the authors as the "Boundary Collocation method" and expresses K_I as a function of the applied force P, the thickness b, and two shape parameters, F_1 and F_2. While F_1 has an analytical expression, the second parameter requires a graph to be obtained. Given the geometric characteristics of the specimen under study and analyzing the graph, it can be verified that F_2 has a value of approximately 0.7 [33].

$$K_I = \frac{P}{b}\sqrt{\alpha}F_1, F_1 = \frac{2(2+\alpha/b)}{(1-\alpha/b)^{\frac{3}{2}}} \frac{1}{\sqrt{a/b}} F_2 \tag{9}$$

A comprehensive comparison between the FEM model's outputs and those of empirical models reveals a remarkable congruence across the entire range of crack lengths, as elucidated in Fig. 14. Strikingly, the maximum absolute difference observed within this analysis was a mere 10 % at the beginning of the propagation when comparing FEM with ASTM E647 standard. This alignment between the FEM and empirical models reinforces the validity of using the FEM approach to simulate fracture mechanics phenomena.

3.2. Experimental tests

In the experimental tests conducted on unmodified specimens CT1 and CT2, two maximum loads (P = 5000 N and P = 6500 N, respectively) were applied to enhance the comparative analysis and select the most suitable crack propagation model. The analysis of Figs. 15 and 16

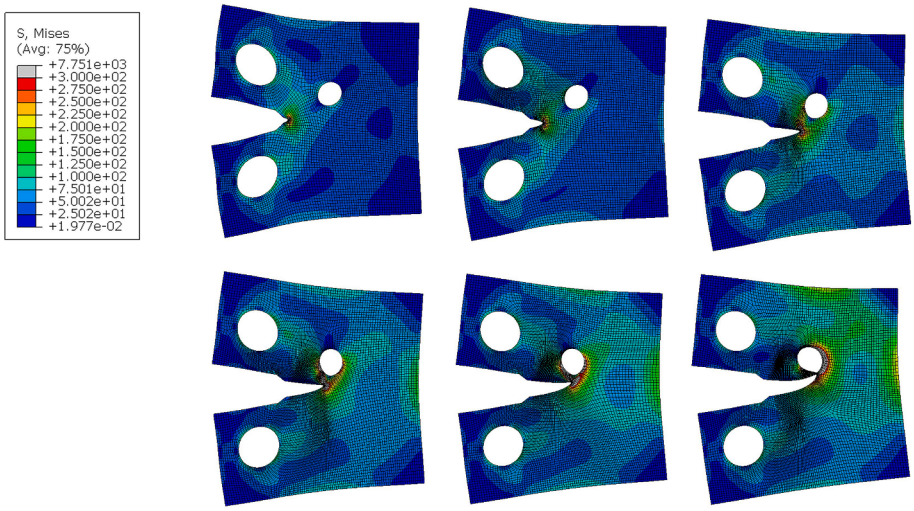

Fig. 12. Example of simulation running the automatic crack propagation algorithm (X_{hole} = 50.5 mm, Y_{hole} = 53.0 mm, R_{hole} = 5 mm).

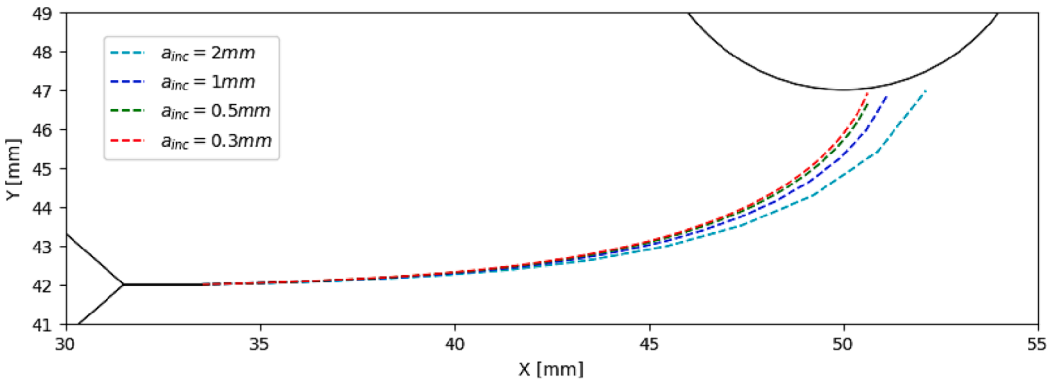

Fig. 13. Trajectories of crack paths using different crack length increments.

Table 8
Performance comparison between simulations with different crack length increments.

a_{inc} [mm]	$X_{intersect}$ [mm]	Variation [mm]	Time (hh:mm:ss)
2.0	52.113	–	(00:03:53)
1.0	51.102	1.011	(00:07:13)
0.5	50.658	0.444	(00:16:25)
0.3	50.623	0.035	(00:30:48)

indicates that the NASGRO model outperforms the other two, with an average error of 13.5 %, while the Paris model exhibits a 52.6 % error, and the Walker model has a 64.6 % error. The NASGRO equation was the only one used in the subsequent steps of the study.

The completion of the experimental procedure, as detailed in the preceding sections, yielded the trajectories for all eight modified specimens. Upon examination of fatigue crack trajectories (Fig. 17 and Table 9), several notable observations can be made. Specimens CT3 to CT9 (Fig. 17 (a)-(g)) exhibit crack behavior consistent with numerical simulations, adhering to the sink/miss hole pattern. In contrast, CT10 (Fig. 17 (h)) deviates from simulation predictions, displaying behavior contrary to the expected additional hole influence.

Among the eight cases, five showcase a maximum deviation under 2 mm, suggesting overall alignment between experimental and simulated outcomes. However, in the case of CT6 (Fig. 17 (d)), the deviation exceeds 2 mm, primarily localized in the final crack section. Yet, excluding this zone, the deviation remains under 2 mm. A similar trend is observed in CT7 (Fig. 17 (e)), where the maximum recorded deviation reaches 4.13 mm. In this instance, the crack tends to rise more than anticipated by the FEM simulations, introducing a notable variation from the predicted behavior.

The spatial distribution of the tested configurations within the additional hole domain is visualized in Fig. 18. This figure also has delineated the sink/miss hole regions, identified through Support Vector Machine techniques, utilizing data derived exclusively from FEM results. Notably, the CT10 case, which yielded an inaccurate prediction, resides near the boundary between the sink/miss hole regions. This boundary was established using numerical data derived from theoretical equations, assuming ideal conditions. However, it is essential to recognize that in practical scenarios, minor perturbations in the test setup or loading conditions may lead to the shifting of this boundary, subsequently impacting the ultimate outcome.

3.3. Machine learning

Each increment's angle predictive model and subsequent crack propagation path were evaluated by comparing its predictions with the experimental outcomes for the predefined test cases (CT4, CT6, and CT8). Various combinations were graphically represented within these domains to facilitate a comprehensive analysis of each model for each approach and test case.

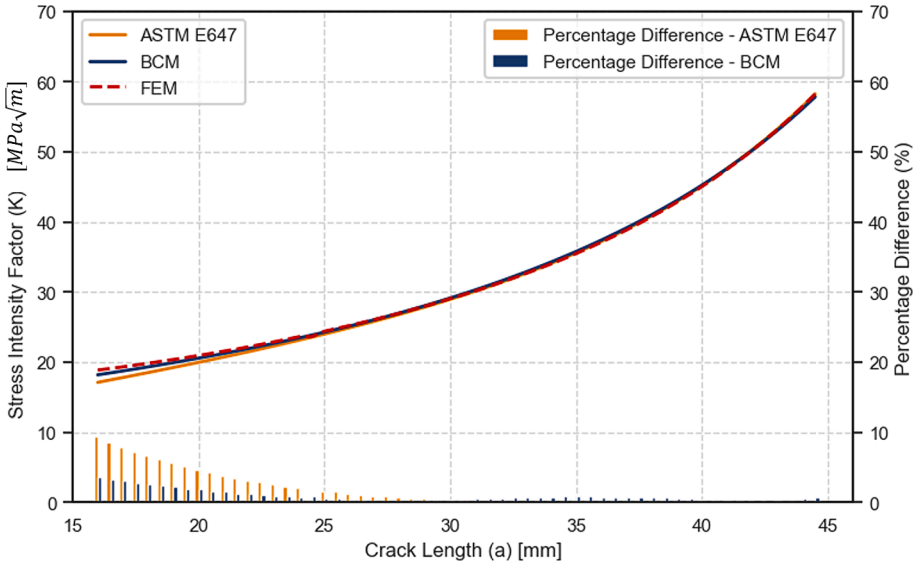

Fig. 14. Comparison of FEM results with empirical models, for an unmodified CT specimen.

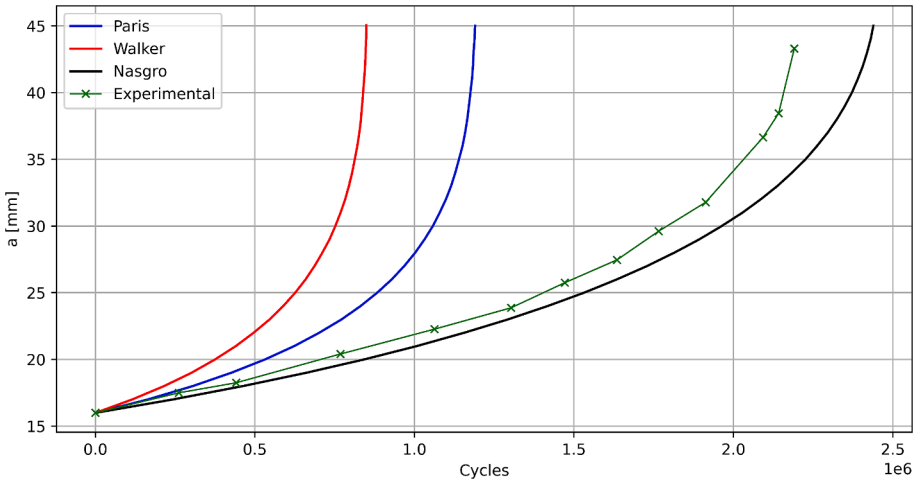

Fig. 15. Fatigue crack propagation curves for CT1 specimen.

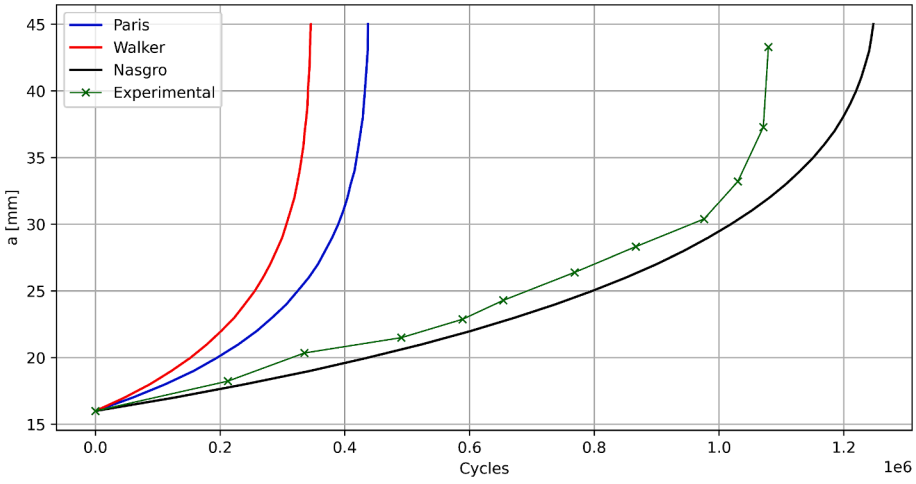

Fig. 16. Fatigue crack propagation curves for CT2 specimen.

3.3.1. Crack propagation

To assess the influence of dataset size, subgroups can be formed: the subgroup with A and B (4 cases), the subgroup with C and D (8 cases), and then each of the approaches E and F (20 and 50 cases, respectively). When comparing the first subgroup (Fig. 19) with more extensive training data set approaches (Fig. 21) it becomes evident that the models' performance improves as the number of cases in the dataset increases. In other words, the predicted trajectories become closer to the experimental ones. Quantitatively, this trend can also be observed in the maximum length deviations, as shown in Table 10, with average deviation values of 2.41 mm, with 4 cases approach, while approach F (with 50 cases) presents an average deviation of 1.19 mm.

On average, the maximum deviation length decreases as the dataset size increases. Although not surprising, it is considered essential to emphasize this conclusion. Additionally, it is worth noting that except for the case of CT6, the increase in dataset size from approach E to F (a 150 % increase) yields insignificant improvements. Nevertheless, it is essential to highlight that, even with a relatively small dataset in machine learning, approaches A and B yield notably good results and are suitable for practical use.

To assess the influence of the data type on performance, a comparison was made between the results of approaches A and B, Fig. 19, and between C and D, Fig. 20. Upon conducting this analysis, it immediately becomes apparent that approaches with purely numerical datasets fail to predict the CT6 case, incorrectly forecasting that the crack will miss the hole, and perform worse in the CT8 case. Conversely, the approaches using experimental data perform worse in the CT4 case. The incorporation of real data into the training datasets leads to significant improvements in predictive performance, even with relatively small datasets. Numerical approaches with sufficiently large datasets also yield high quality predictions.

Different authors have analyzed crack propagation on modified CT specimens using FEM and ML. Originally experimentally analyzed by Miranda et al. [34] this specimen configuration is accurately simulated using the MTS criterion [35,36] or more recently with the VCTD criterion by Baptista et al. [19]. While the MTS criterion is widely accepted the VCTD criterion can be used with more complex material models, as it is not limited to linear elastic models [8]. Both allowed for accurate fatigue crack propagation paths. Using ML tools both Baptista et al. [19] and Wang et al. [3] have used ANN and RBFN to simulate crack propagation on modified CT specimens, and were able to predict hole behavior. The results presented in this paper show improved results by the use of deep learning tools. Regarding experimental results, in 2015 Lu et al. [37] analyzed an Al 7075-T6 specimen with a 5 mm diameter hole and 50 mm width. Different behaviors were found for holes located at 9 mm from the specimen central line (sinkhole) and 12 mm (miss-hole), which is in line with this papers' obtained results. These authors also analyze the specimen behavior under constant and variable load amplitudes, concluding that the crack propagation path is not affected by the loading nature. Therefore, one can consider the numerical

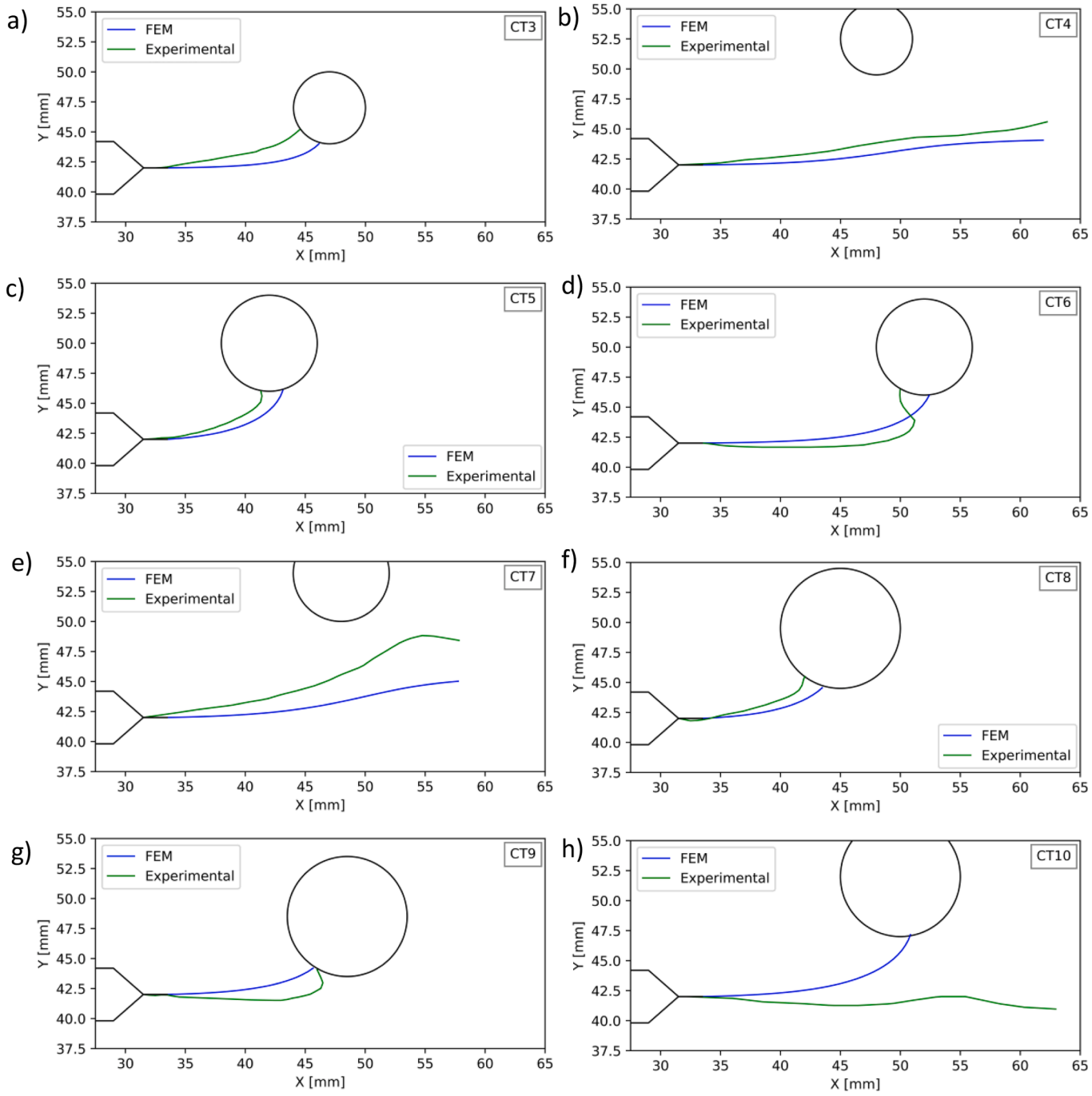

Fig. 17. Experimental and FEM trajectories of modified CT specimens: a) CT3, b) CT4, c) CT5, d) CT6, e) CT7, f) CT8, g) CT9 and h) CT10.

Table 9
Maximum deviation length for CT3 to CT10 specimens.

Specimen	CT3	CT4	CT5	CT6	CT7	CT8	CT9	CT10
Max. deviation length [mm]	1.99	1.42	1.62	2.36	4.13	1.17	1.94	–

approach in this paper to be valid.

The kNN method is significantly influenced by the size of the dataset, as there is no training process to enhance predictive capabilities. This trend can be depicted in the results obtained for approaches with only 4 cases (Fig. 22), failing to forecast two out of six and showing poor performance in the remaining.

When transitioning to approaches with 8 cases (Fig. 23) an improvement in path prediction is observed, sustained by a reduction in the maximum deviation error, presented in Table 11.

Finally, despite the increase from 8 to 20 cases, approach E does not exhibit improvements over approach D, with average deviations of 1.69 mm and 1.75 mm respectively. However, considering approach F with 50 cases, superior performance is observed. The predicted trajectories of these last two approaches can be visualized in Fig. 24.

In this method, introducing experimental data in the dataset leads to poorer results. This is evident when comparing approaches A and B, in which the purely experimental approach completely fails in 2 out of the 3 test cases. Similarly, when comparing approaches C and D, the one containing experimental data fails in one case and exhibits worse performance than the purely numerical approach.

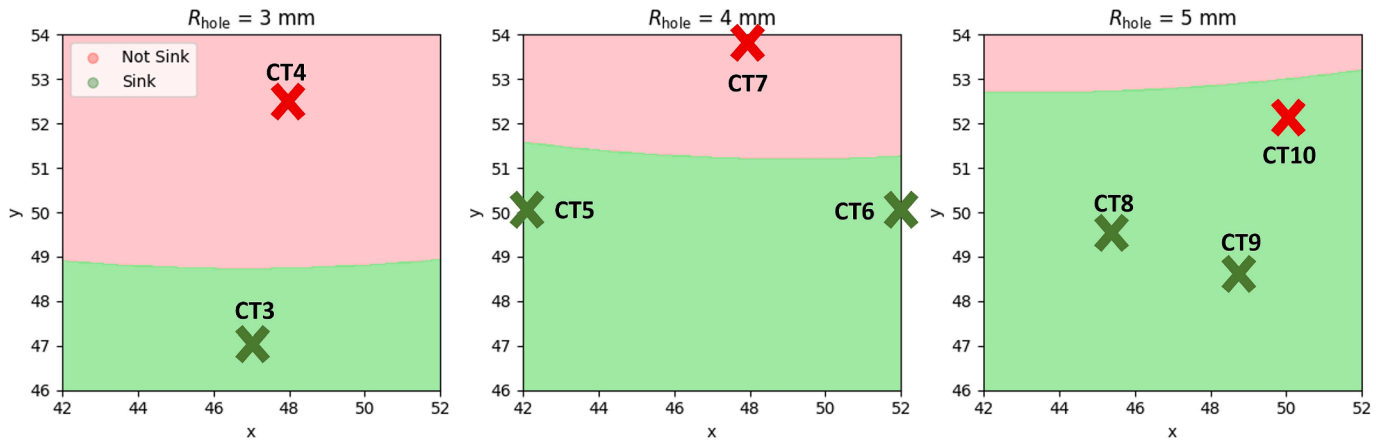

Fig. 18. Sink or miss hole regions for radii of 3 mm, 4 mm and 5 mm.

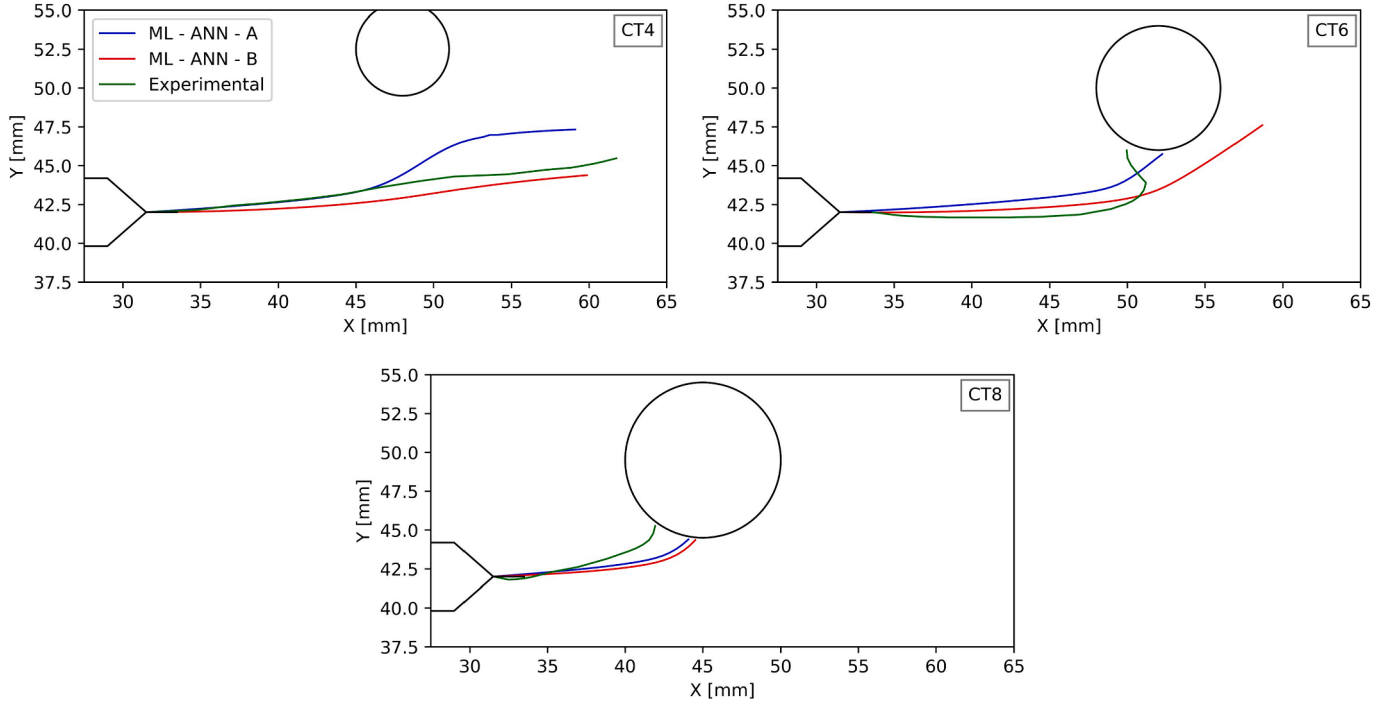

Fig. 19. Trajectories of test CT specimens regarding experimental and ANN approaches A and B.

Table 10
Maximum deviation length between experimental and ANN trajectories.

	A [mm]	B [mm]	C [mm]	D [mm]	E [mm]	F [mm]
CT4	2.63	0.91	2.41	0.36	0.60	0.37
CT6	2.63	–	2.07	–	3.56	1.90
CT8	1.96	2.28	1.15	1.55	1.34	1.30
Average	2.41	–	1.88	–	1.83	1.19

In summary, larger datasets favor ANN and kNN methods, showcasing similar performance. In contrast, for smaller datasets, particularly in approaches A, B, C, and D, ANN outperforms kNN, aligning with expectations due to kNN's reliance on dataset size. Additionally, ANN excels at handling experimental data with real-world noise, which challenges kNN's capabilities.

According to Mortazavi et al., higher value variables can skew the weight and bias of ANN and kNN parameters while training occur [4]. Therefore, the normalization step was fundamental, as crack deflection is dictated by the K_{II} value, which is much lower than the K_I value in the current mixed mode problem [10,38]. Some authors go as far as taking the logarithmic value of input variables before normalization to reduce this problem even further [39]. Gope et al. [15] and Giannella et al. [40] also mention that the ML model structure is very important to avoid over and underfitting problems. Both the activation functions between ANN hidden layers and the number of neurons can significantly affect the network performance. Giannella et al compare different networks architectures with different activation functions, number of neurons and dropout percentages between layers. These authors concluded that shallow networks can be better when only a few points are available for training, but at least 10 % of dropout is required when a large amount of data is available, in order to avoid instability problems.

Finally, computational time comparisons, presented on Table 12, reveal that, regarding the simulation of ten configurations, using ANN represents a reduction of 94 % of computational time and more than 99.95 % in the case of kNN.

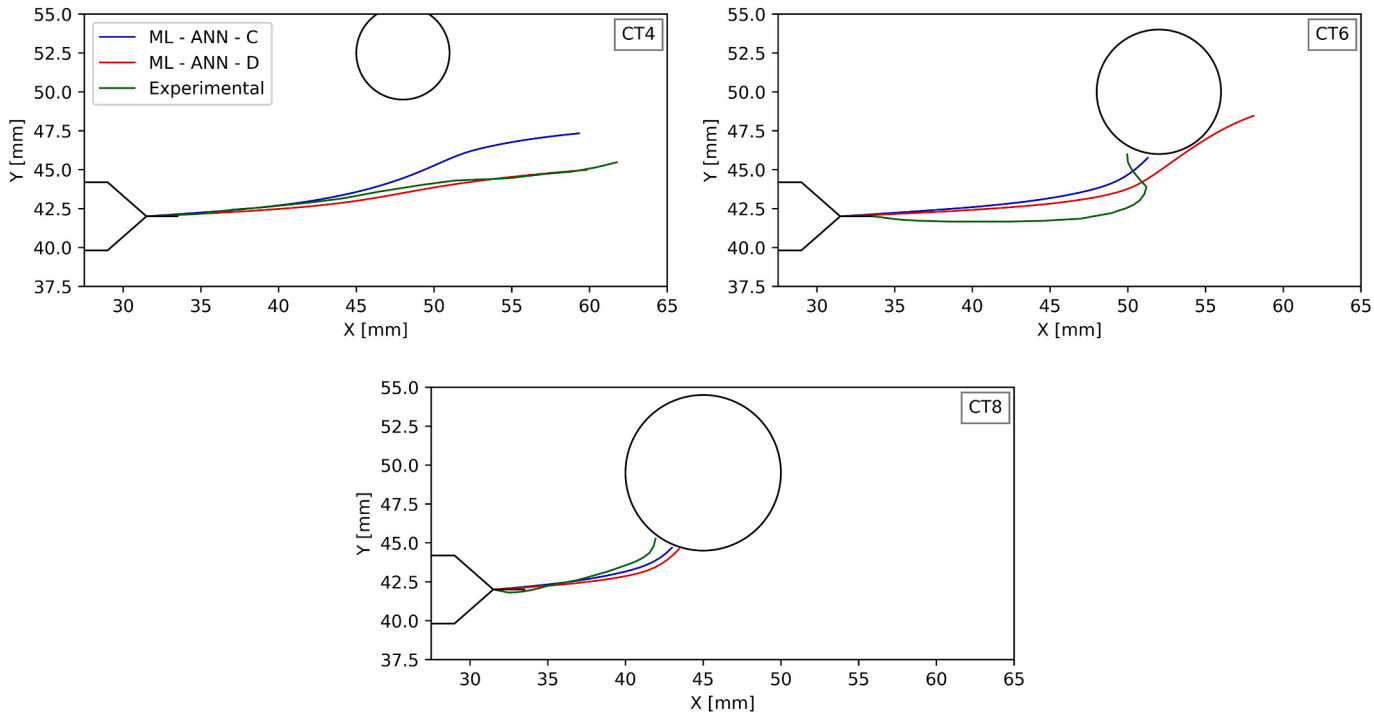

Fig. 20. Trajectories of test CT specimens regarding experimental and ANN approaches C and D.

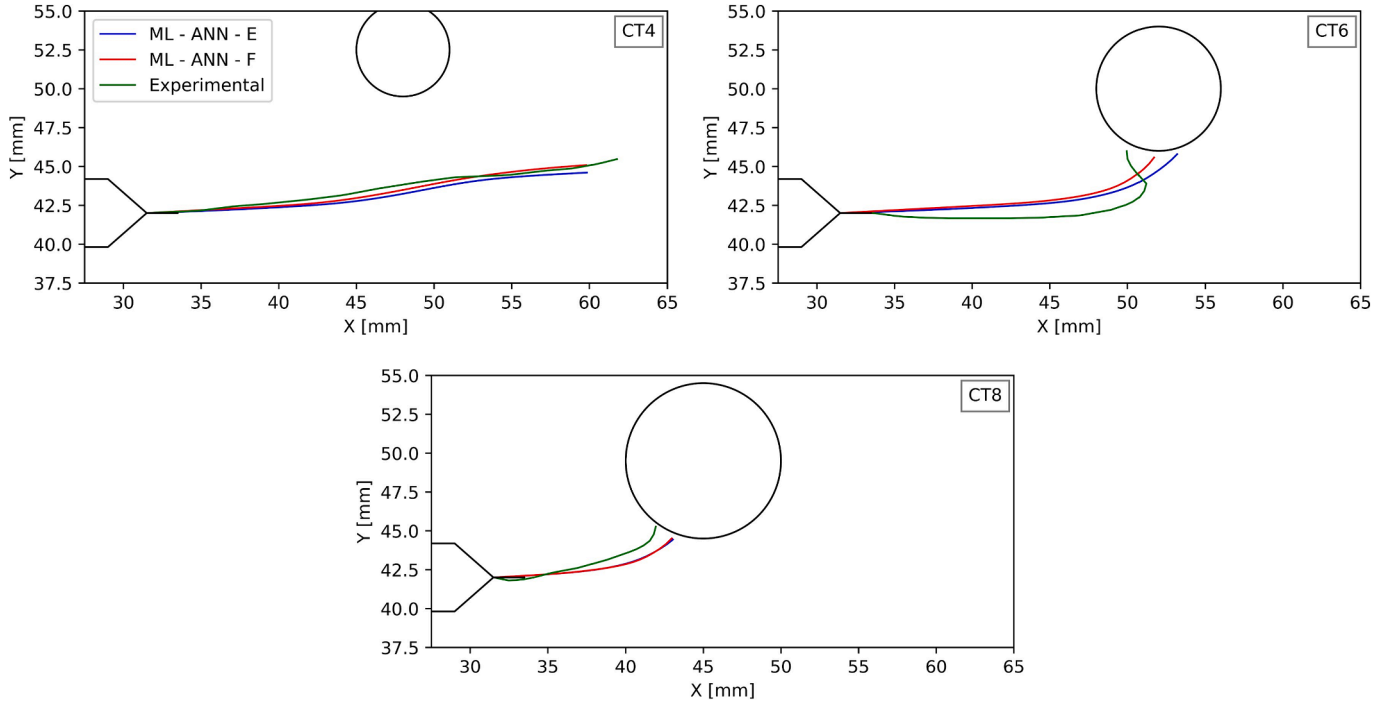

Fig. 21. Trajectories of test CT specimens regarding experimental and ANN approaches E and F.

3.3.2. *Fatigue life*

The evaluation of the implemented fatigue life prediction models was divided into two parts: first, their performance in predicting K_I values with respect to crack length for different configurations was assessed. Then, these models were used to incorporate a variable amplitude fatigue crack growth algorithm, enabling the prediction of crack propagation curves as a function of applied cycles for seven experimental cases.

Figs. 25 and 26 show K_I predictions for two configurations alongside with FEM values, serving as the ground truth. The relative errors are represented as bar charts at each point on the K_I curves.

Both methods generally predict K_I accurately as a function of crack length, with errors typically below 10 %. ANN tends to overestimate for initial crack lengths (under 23 mm), while kNN excels in the initial region. However, the performance reverses beyond 22 mm, with ANN providing more accurate predictions than kNN. For the case where the crack converges to the hole (Fig. 26), both methods exhibit significant deviations in the last 2 mm, resulting in substantial errors (22 % for the

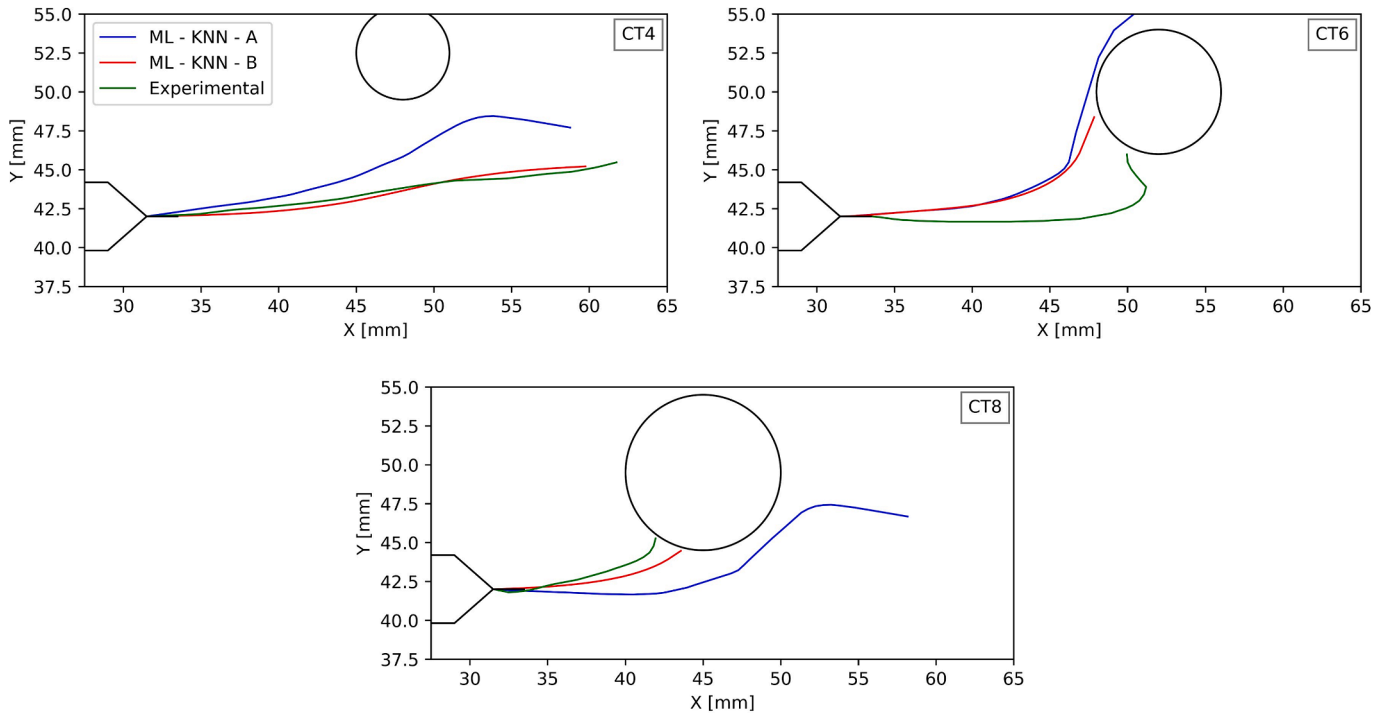

Fig. 22. Trajectories of test CT specimens regarding experimental and KNN approaches A and B.

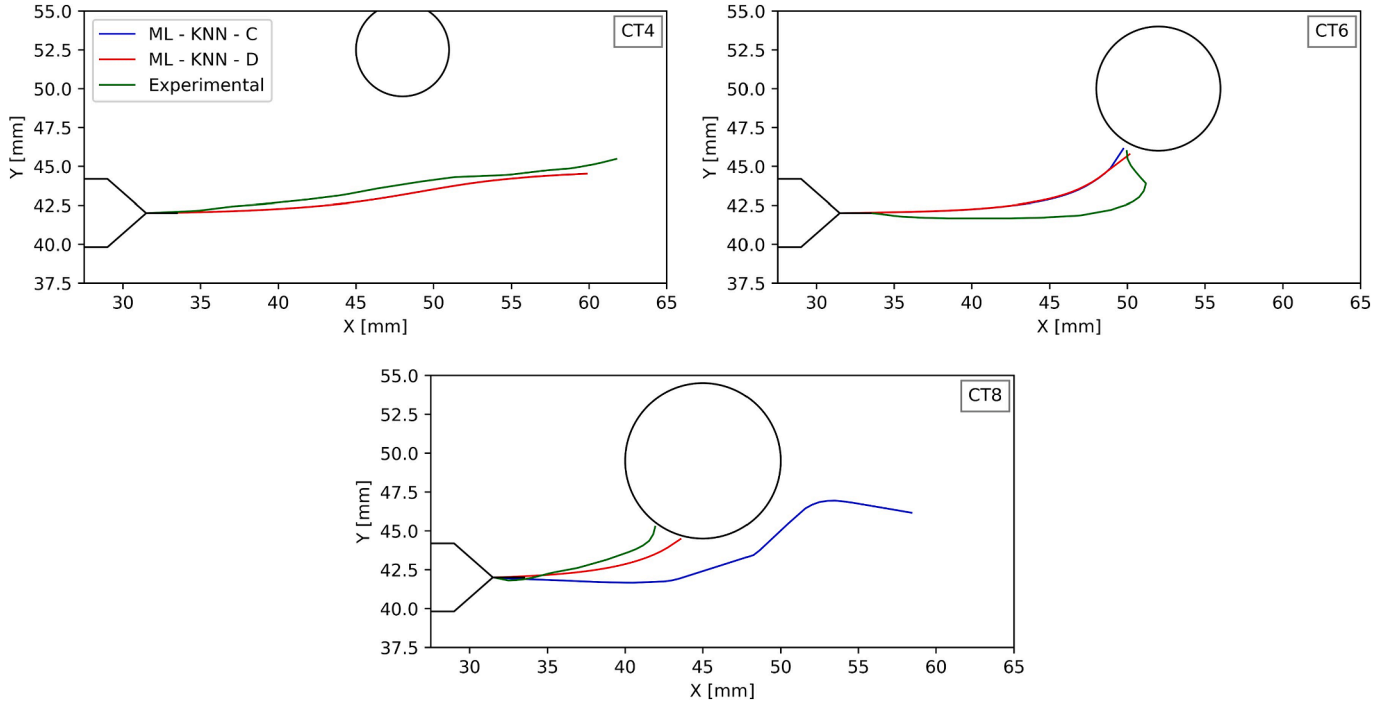

Fig. 23. Trajectories of test CT specimens regarding experimental and KNN approaches C and D.

Table 11
Maximum deviation length between experimental and kNN trajectories.

	A [mm]	B [mm]	C [mm]	D [mm]	E [mm]	F [mm]
CT4	4.13	0.4	0.66	0.66	0.86	0.85
CT6	–	6.41	3.3	2.83	3.84	1.82
CT8	–	1.57	–	1.57	0.56	0.64
Average	–	2.79	–	1.69	1.75	1.10

final length). The best agreement between ML and FEM is observed when the crack diverges from the hole (Fig. 25), with slight discrepancies: kNN slightly overestimates, while ANN undervalues.

Regarding fatigue life, the implemented methods were used to predict the fatigue life and crack propagation curves for the tested specimens. In general, as presented in Table 13, both methods provided reasonably accurate predictions for cases where the crack did not converge to the additional hole (example Fig. 27), with errors less than 2 %.

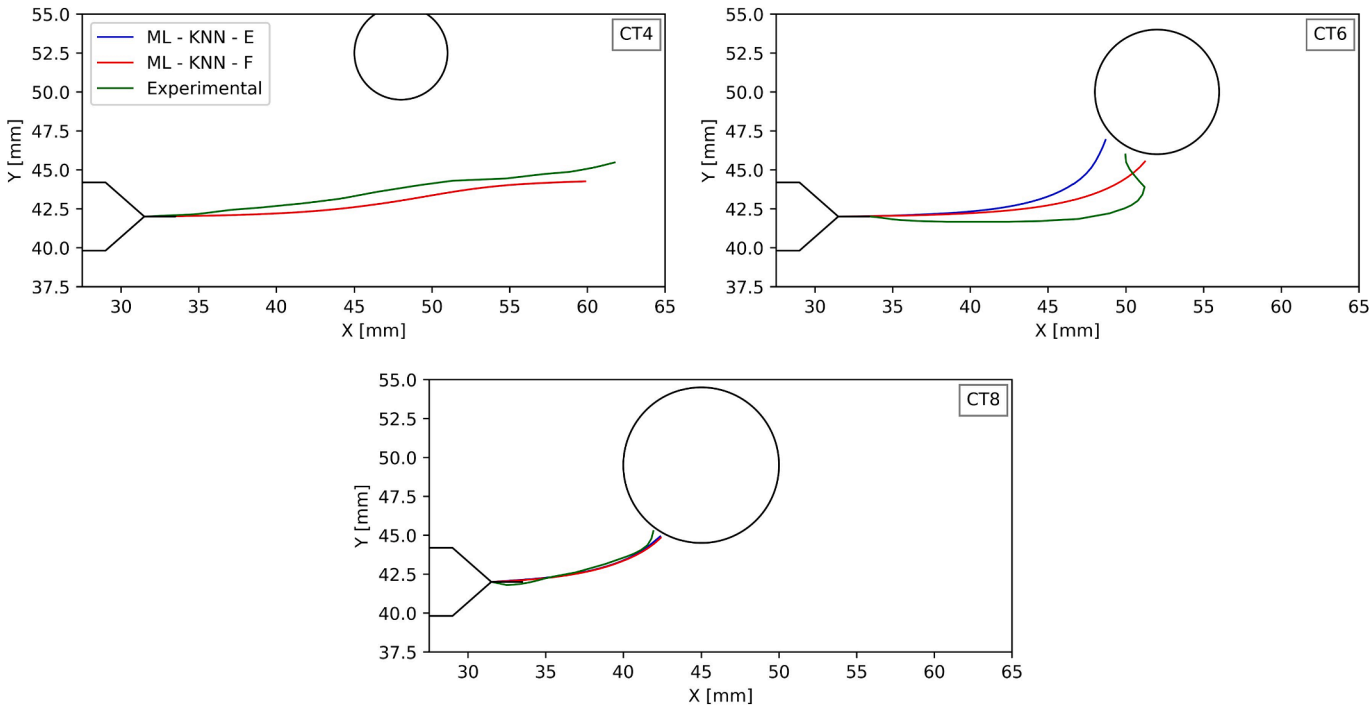

Fig. 24. Trajectories of test CT specimens regarding experimental and kNN approaches E and F.

Table 12
Computational time per simulation of FEM, ANN and kNN for different number of simulations.

Simulations	FEM	Methods ANN	kNN
1	(00:16:25)	(00:05:31)	<(00:00:01)
10	(02:44:10)	(00:09:51)	(00:00:04)

However, for cases where the crack converged to the hole (example Fig. 28), the predictions were less accurate, with errors reaching approximately 45 %. ANN models exhibited better accuracy compared to kNN. For the seven specimens, ANN had an average error of 10.1 %, while kNN showed 16.7 %.

4. Conclusions

The study achieved several key findings that enhance the understanding of fatigue crack propagation and the application of machine learning (ML) techniques in fracture mechanics. Firstly, the MTS criterion combined with Finite Element Method (FEM) yielded promising results, with seven out of eight specimens demonstrating well-predicted behavior in experimental tests. However, challenges were observed in predicting FCG under variable amplitude conditions, highlighting the importance of selecting appropriate algorithms such as the NASGRO model. The subsequent application of ML underscored the significance of data preprocessing techniques, particularly Feature Engineering, in improving prediction accuracy.

Furthermore, the influence of dataset size on prediction accuracy

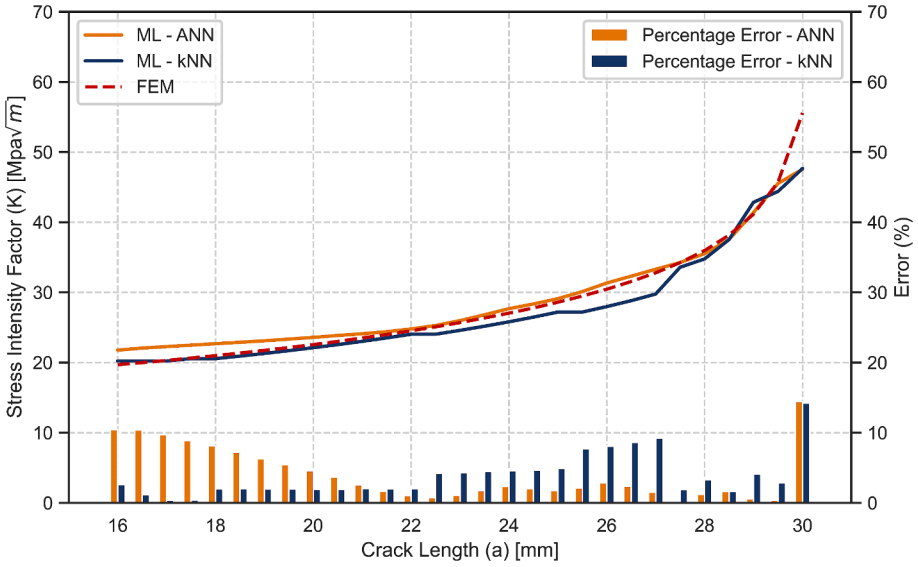

Fig. 25. Results of KI over a prediction for test 1 and comparison with FEM.

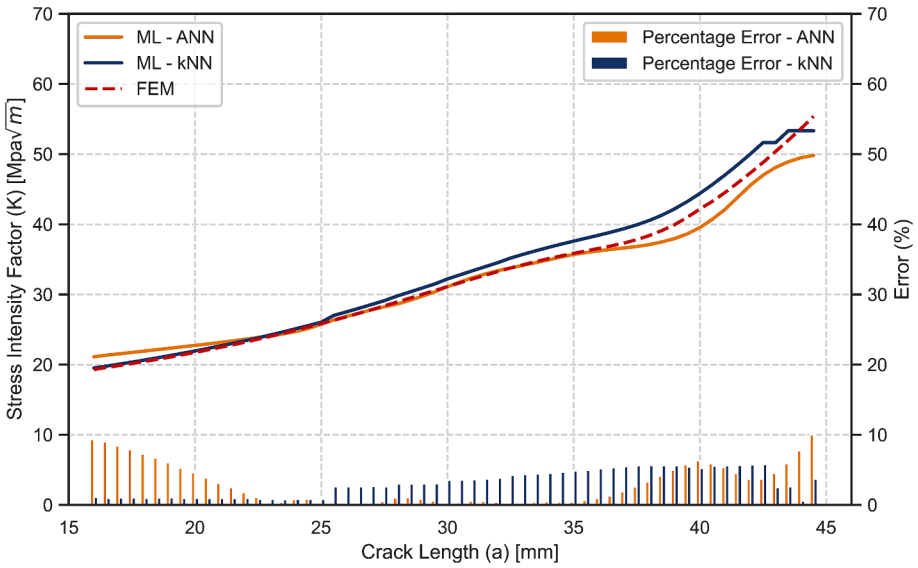

Fig. 26. Results of KI over a prediction for test 2 and comparison with FEM.

Table 13
Number of cycles until failure: experimental and machine learning predictions.

	Experimental	ANN		KNN	
		Cycles	Diff. [%]	Cycles	Diff. [%]
CT3	572 250	615 171	7.5	717 957	25.5
CT4	1 057 845	1 062 950	0.5	1 038 453	1.8
CT5	387 495	572 584	47.8	549 596	41.8
CT6	825 675	819 470	0.8	956 729	15.9
CT7	1 005 525	1 015 550	1.0	987 648	1.8
CT8	392 400	442 065	12.7	482 748	23.0
CT9	524 835	525 727	0.2	561 301	6.9
		Average	10.1	**Average**	16.7

was investigated, with both ANN and kNN models demonstrating varying performance depending on the dataset size. While ANN could yield acceptable results with smaller datasets, kNN required larger datasets to achieve comparable performance. Additionally, the comparison between ANN and kNN revealed differences in computational efficiency, with ANN outperforming kNN in terms of prediction accuracy but at the cost of higher computational time.

Overall, the study highlights the potential of ML in fracture mechanics, particularly in predicting fatigue crack propagation and component service life. Despite identified limitations, such as the dependency on large datasets and sensitivity to data quality, ML offers significant advantages, including a substantial reduction in computational costs. Moving forward, further research in this area could explore more complex ML models and address the identified limitations to enhance the predictive capabilities of ML in fracture mechanics applications.

CRediT authorship contribution statement

B. Santos: Conceptualization, Formal analysis, Investigation, Methodology, Visualization, Writing – original draft. **V. Infante:** Conceptualization, Methodology, Supervision, Validation, Writing – review & editing. **T. Barros:** Conceptualization, Methodology, Supervision, Validation, Writing – review & editing. **R. Baptista:** Writing – review & editing, Validation, Supervision, Methodology, Investigation.

Declaration of competing interest

The authors declare that they have no known competing financial interests or personal relationships that could have appeared to influence the work reported in this paper.

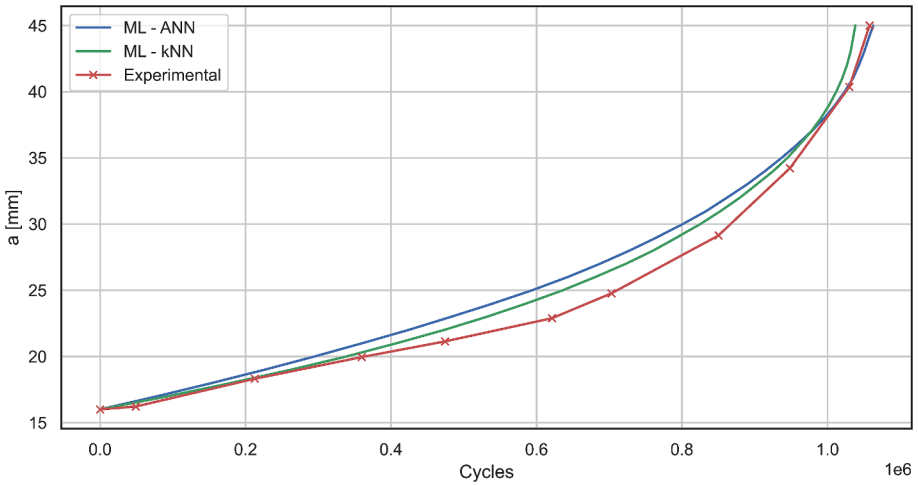

Fig. 27. Fatigue crack propagation curves for CT4 specimen.

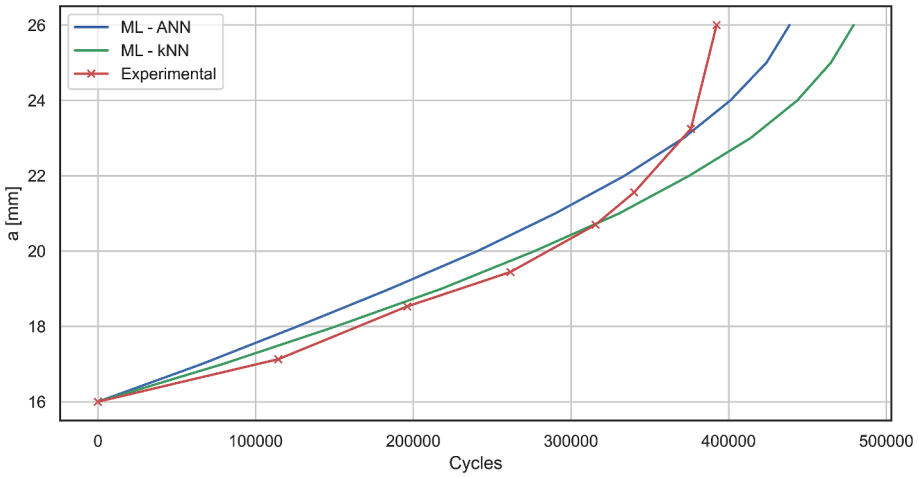

Fig. 28. Fatigue crack propagation curves for CT8 specimen.

Data availability

No data was used for the research described in the article.

Acknowledgements

This work was supported by Fundação para a Ciência e Tecnologia (FCT), through IDMEC under LAETA (UIDB/50022/2020) and C-MAST (UIDB/00151/2020).

References

[1] Bhaumik SK, Sujata M, Venkataswamy MA. Fatigue failure of aircraft components. Eng Fail Anal Sep. 2008;15(6):675–94. https://doi.org/10.1016/j.engfailanal.2007.10.001.
[2] Wang H, Li B, Gong J, Xuan F-Z. Machine learning-based fatigue life prediction of metal materials: Perspectives of physics-informed and data-driven hybrid methods. Eng Fract Mech May 2023;284:109242. https://doi.org/10.1016/j.engfracmech.2023.109242.
[3] Wang B, Xie L, Song J, Zhao B, Li C, Zhao Z. Curved fatigue crack growth prediction under variable amplitude loading by artificial neural network. Int J Fatigue Jan. 2021;142:105886. https://doi.org/10.1016/j.ijfatigue.2020.105886.
[4] R. Plank and G. Kuhn, "Fatigue crack propagation under non-proportional mixed mode loading.".
[5] Baptista R, Infante V, Madeira JFA. Optimization of a cruciform specimen for fatigue crack growth under in and out-of-phase in-plane biaxial loading conditions. Mech Adv Mater Struct Mar. 2023;30(8):1649–66. https://doi.org/10.1080/15376494.2022.2038740.
[6] Giannella V, Dhondt G, Kontermann C, Citarella R. Combined static-cyclic multi-axial crack propagation in cruciform specimens. Int J Fatigue Jun. 2019;123:296–307. https://doi.org/10.1016/j.ijfatigue.2019.02.029.
[7] Ayatollahi MR, Razavi N, Yahya MY. Mixed mode fatigue crack initiation and growth in a CT specimen repaired by stop hole technique. Eng Fract Mech Aug. 2015;145:115–27. https://doi.org/10.1016/j.engfracmech.2015.03.027.
[8] Floros D, Ekberg A, Larsson F. Evaluation of crack growth direction criteria on mixed-mode fatigue crack growth experiments. Int J Fatigue Dec. 2019;129. https://doi.org/10.1016/j.ijfatigue.2019.04.013.
[9] Antunes FV, Branco R, Ferreira JAM, Borrego LP. Stress intensity factor solutions for CTS mixed mode specimen. Frattura ed Integrita Strutturale Apr. 2019;13(48):676–92. https://doi.org/10.3221/IGF-ESIS.48.64.
[10] Shi J, Chopp D, Lua J, Sukumar N, Belytschko T. Abaqus implementation of extended finite element method using a level set representation for three-dimensional fatigue crack growth and life predictions. Eng Fract Mech Sep. 2010;77(14):2840–63. https://doi.org/10.1016/j.engfracmech.2010.06.009.
[11] Baptista R, Marques J, Infante V. Algorithm for automatic fatigue crack growth simulation on welded high strength steels. Frattura ed Integrita Strutturale Apr. 2019;13(48):257–68. https://doi.org/10.3221/IGF-ESIS.48.27.
[12] Wang H, Zhang W, Sun F, Zhang W. A Comparison Study of Machine Learning Based Algorithms for Fatigue Crack Growth Calculation. Materials May 2017;10(5):543. https://doi.org/10.3390/ma10050543.
[13] Mortazavi SNS, Ince A. An artificial neural network modeling approach for short and long fatigue crack propagation. Comput Mater Sci Dec. 2020;185:109962. https://doi.org/10.1016/j.commatsci.2020.109962.
[14] Liu X, Athanasiou CE, Padture NP, Sheldon BW, Gao H. A machine learning approach to fracture mechanics problems. Acta Mater May 2020;190:105–12. https://doi.org/10.1016/j.actamat.2020.03.016.
[15] Gope D, Gope PC, Thakur A, Yadav A. Application of artificial neural network for predicting crack growth direction in multiple cracks geometry. Appl Soft Comput May 2015;30:514–28. https://doi.org/10.1016/j.asoc.2015.02.003.
[16] Liu Y-K, Fan J-L, Zhu G, Zhu M-L, Xuan F-Z. Data-driven approach to very high cycle fatigue life prediction. Eng Fract Mech Nov. 2023;292:109630. https://doi.org/10.1016/j.engfracmech.2023.109630.
[17] Zhao Y, Liu Y, Xu Z. Statistical learning prediction of fatigue crack growth via path slicing and re-weighting. Theor Appl Mech Lett 2023;13(6):Nov. https://doi.org/10.1016/j.taml.2023.100477.
[18] Perera R, Guzzetti D, Agrawal V. Graph neural networks for simulating crack coalescence and propagation in brittle materials. Comput Methods Appl Mech Eng May 2022;395:115021. https://doi.org/10.1016/j.cma.2022.115021.
[19] Baptista R, Moita P, Infante V. Fatigue crack growth on modified CT specimens using artificial neural networks. Int J Fatigue Feb. 2023;167:107357. https://doi.org/10.1016/j.ijfatigue.2022.107357.
[20] Liang W, Lou M, Wang Y, Zhang C, Chen S, Cui C. A fatigue crack growth prediction method on small datasets based on optimized deep neural network and Delaunay data augmentation. Theor Appl Fract Mech Feb. 2024;129. https://doi.org/10.1016/j.tafmec.2023.104218.
[21] Chen D, Li Y, Liu K, Li Y. A physics-informed neural network approach to fatigue life prediction using small quantity of samples. Int J Fatigue Jan. 2023;166. https://doi.org/10.1016/j.ijfatigue.2022.107270.
[22] Fan J-L, Zhu G, Zhu M-L, Xuan F-Z. A data-physics integrated approach to life prediction in very high cycle fatigue regime. Int J Fatigue Nov. 2023;176:107917. https://doi.org/10.1016/j.ijfatigue.2023.107917.
[23] Do DTT, Lee J, Nguyen-Xuan H. Fast evaluation of crack growth path using time series forecasting. Eng Fract Mech Sep. 2019;218. https://doi.org/10.1016/j.engfracmech.2019.106567.
[24] Han S, Khatir S, Abdel Wahab M. A deep learning approach to predict fretting fatigue crack initiation location. Tribol Int 2023;185:Jul. https://doi.org/10.1016/j.triboint.2023.108528.
[25] Long X, Ding X, Jiang C, Zhang X, Liao W, Liu K. An intelligent crack damage assessment method by integrating information and physics. Eng Fract Mech Jan. 2024;295:109737. https://doi.org/10.1016/j.engfracmech.2023.109737.
[26] "Standard Test Method for Measurement of Fatigue Crack Growth Rates", doi: 10.1520/E0647-13A.
[27] T. Barros, "Previsão do tempo de vida de fadiga da aeronave Epsilon TB-30 baseada em ensaios experimentais representativos da operação da aeronave em provetes que simulam as zonas críticas.".
[28] Barros T, et al. Fatigue failure analysis on the 2nd bulkhead beam of the Portuguese Air Force Epsilon TB-30 aircraft. Eng Fail Anal Sep. 2023;151:107404. https://doi.org/10.1016/j.engfailanal.2023.107404.
[29] N. E. Dowling, *Mechanical Behavior of Materials*, Fourth. Pearson.
[30] S., A. S., A. A. Beden. Review of Fatigue Crack Propagation Models for Metallic Components. Eur J Sci Res 2009:364–97.
[31] J. Harter, "AFGROW user guide and technical manual," 1999.
[32] Martins T, Baptista R, Infante V, Sousa L, Antunes PJ, Serrano B. Numerical study of the Epsilon TB30 aircraft frame. Eng Fail Anal Nov. 2020;117:104966. https://doi.org/10.1016/j.engfailanal.2020.104966.
[33] Tada H, Paris PC, Irwin GR. The Stress Analysis of Cracks Handbook. *Third Edition* ASME Press 2000. https://doi.org/10.1115/1.801535.
[34] Miranda ACO, Meggiolaro MA, Castro JTP, Martha LF, Bittencourt TN. Fatigue life and crack path predictions in generic 2D structural components. Eng Fract Mech 2003;70(10):1259–79. https://doi.org/10.1016/S0013-7944(02)00099-1.
[35] Ali Fageehi Y. Prediction of Fatigue Crack Growth Rate and Stress Intensity Factors Using the Finite Element Method. Adv Mater Sci Eng 2022, 2022,. https://doi.org/10.1155/2022/2705240.
[36] Alshoaibi AM, Fageehi YA. Numerical analysis of fatigue crack growth path and life predictions for linear elastic material. Materials Aug. 2020;13(15):1–15. https://doi.org/10.3390/ma13153380.

[37] Z. Lu, J. Xu, L. Wang, J. Zhang, and Y. Liu, "Curvilinear Fatigue Crack Growth Simulation and Validation under Constant Amplitude and Overload Loadings," *J Aerosp Eng*, vol. 28, no. 1, Jan. 2015, doi: 10.1061/(ASCE)AS.1943-5525.0000337.
[38] A. M. Alshoaibi, "Computational simulation of 3D fatigue crack growth under mixed-mode loading," *Applied Sciences (Switzerland)*, vol. 11, no. 13, Jul. 2021, doi: 10.3390/app11135953.
[39] J. F. Barbosa, J. A. F. O. Correia, R. C. S. F. Júnior, and A. M. P. De esus, "Fatigue life prediction of metallic materials considering mean stress effects by means of an artificial neural network," *Int J Fatigue*, vol. 135, Jun. 2020, doi: 10.1016/j.ijfatigue.2020.105527.
[40] Giannella V, Bardozzo F, Postiglione A, Tagliaferri R, Sepe R, Armentani E. Neural networks for fatigue crack propagation predictions in real-time under uncertainty. Comput Struct Nov. 2023;288. https://doi.org/10.1016/j.compstruc.2023.107157.